THE PLANT CELL

The Plant Cell, 2025, **37**, koae280
https://doi.org/10.1093/plcell/koae280
Advance access publication 15 October 2024
Research Article

TYPHON proteins are RAB-dependent mediators of the *trans*-Golgi network secretory pathway

Anirban Baral,[1,*,†] Delphine Gendre,[1,†] Bibek Aryal,[1] Louise Fougère,[2] Luciano Martin Di Fino,[1] Chihiro Ohori,[3] Bernadette Sztojka,[1] Tomohiro Uemura,[3] Takashi Ueda,[4,5] Peter Marhavý,[1] Yohann Boutté,[2,*] Rishikesh P. Bhalerao[1,*]

[1]Department of Forest Genetics and Plant Physiology, Umeå Plant Science Centre, Swedish University of Agricultural Sciences, Umeå 901 87, Sweden
[2]Laboratoire de Biogénèse Membranaire, UMR5200, Université de Bordeaux, CNRS, Villenave d'Ornon 33140, France
[3]Natural Science Division, Faculty of Core Research, Ochanomizu University, Tokyo 112-8610, Japan
[4]Division of Cellular Dynamics, National Institute for Basic Biology, Okazaki, Aichi 444-8585, Japan
[5]The Department of Basic Biology, SOKENDAI (The Graduate University for Advanced Studies), Okazaki, Aichi 444-8585, Japan
*Author for correspondence: abaral1986@gmail.com (A.B), yohann.boutte@u-bordeaux.fr (Y.B), rishi.bhalerao@slu.se (R.P.B)
†These authors contributed equally to this work.
The author responsible for distribution of materials integral to the findings presented in this article in accordance with the policy described in the Instructions for Authors (https://academic.oup.com/plcell/pages/General-Instructions) is Rishikesh P. Bhalerao (rishi.bhalerao@slu.se)

Abstract

The *trans*-Golgi network (TGN), a key compartment in endomembrane trafficking, participates in both secretion to and endocytosis from the plasma membrane. Consequently, the TGN plays a key role in plant growth and development. Understanding how proteins are sorted for secretion or endocytic recycling at the TGN is critical for elucidating mechanisms of plant development. We previously showed that the protein ECHIDNA is essential for phytohormonal control of hypocotyl bending because it mediates secretion of cell wall components and the auxin influx carrier AUXIN RESISTANT 1 (AUX1) from the TGN. Despite the critical role of ECHIDNA in TGN-mediated trafficking, its mode of action remains unknown in Arabidopsis (*Arabidopsis thaliana*). We therefore performed a suppressor screen on the *ech* mutant. Here, we report the identification of TGN-localized TYPHON 1 (TPN1) and TPN2 proteins. A single amino acid change in either TPN protein causes dominant suppression of the *ech* mutant's defects in growth and AUX1 secretion, while also restoring wild-type (WT)-like ethylene-responsive hypocotyl bending. Importantly, genetic and cell biological evidence shows that TPN1 acts through RAS-ASSOCIATED BINDING H1b (RABH1b), a TGN-localized RAB-GTPase. These results provide insights into ECHIDNA-mediated secretory trafficking of cell wall and auxin carriers at the TGN, as well as its role in controlling plant growth.

Introduction

The *trans*-Golgi network (TGN) is a multifunctional organelle in the plant endomembrane system that mediates secretion of newly synthesized proteins to the plasma membrane (PM) and vacuole as well as endocytic recycling (Viotti et al. 2010; Feraru et al. 2012; Rosquete et al. 2018; Shimizu et al. 2021). To fully understand the mechanisms of plant development and adaptation to environmental signals, it is vital to understand how membrane trafficking is coordinated in this compartment. Genetic and cell biological analyses of the model plant Arabidopsis (*Arabidopsis thaliana*) have shown that TGN-mediated secretion plays a major role in plant morphogenesis by enabling the trafficking of key regulators of polar auxin transport such as (PIN-FORMED) PIN and AUXIN RESISTANT/LIKE AUXIN RESISTANT (AUX/LAX) proteins (Boutté et al. 2013; Tanaka et al. 2013) as well as cell wall components such as pectin and xyloglucans (Wang et al. 2017; Wilkop et al. 2019). We have previously identified the protein ECHIDNA (ECH) as a key mediator of the TGN's secretory functions (Gendre et al. 2011). Loss of ECH causes dramatic defects in the TGN ultrastructure and defective secretion of the cell wall components hemicellulose and pectin as well as the auxin transporter AUX1 (Boutté et al. 2013; Gendre et al. 2013). In keeping with the key role of secretion in cell elongation, the *ech* mutant displays defects in cell elongation that lead to stunted root, hypocotyl, and rosette growth (Gendre et al. 2011). Importantly, formation of the apical hook, a bend formed by differential cell elongation on either side of the hypocotyl of germinating seeds, which is required for soil emergence, is severely abrogated in *ech* (Boutté et al. 2013). Loss of ECH results in mislocalization of a subset of TGN-localized proteins such as SYNTAXIN OF PLANTS 61 (SYP61) or Vacuolar H(+)-ATPase subunit a isoform 1 (VHAa1) but has minimal effect on other TGN proteins such as the clathrin heavy chain (CHC) (Boutté et al. 2013), or the EPSIN N-terminal homology (ENTH) proteins EPSIN1 and MODIFIED TRANSPORT TO THE VACUOLE1 (MTV1) which are involved in vacuolar trafficking (Heinze et al. 2020). Consistently, while trafficking of lytic vacuole-targeted proteins is unaffected in *ech* mutant (Gendre et al. 2011), PM-targeted AUX1 and cargoes destined for the cell wall (e.g. xyloglucans) are mislocalized to vacuoles in *ech* (Boutté et al. 2013; McFarlane et al. 2013). In spite of these key functions at the TGN, the ECH-mediated molecular mechanisms of cargo sorting at TGN remain elusive. Biochemical and genetic studies showed that ECH forms a complex with the YPT/RAB-GTPase interacting proteins (YIPs) YIP4a and YIP4b, which localize to the TGN (Gendre et al. 2013). Moreover, the microtubule binding protein TGN-ASSOCIATED PROTEIN 1 (TGNap1) has been shown to interact

Received May 14, 2024. Accepted October 9, 2024

both with YIP proteins and the RAB-GTPase RAS-ASSOCIATED BINDING H1b (RABH1b) (Renna et al. 2018). Nonetheless, it is still not clear how the TGN coordinates the sorting of proteins into diverse secretory pathways and how specificity in trafficking of PM-localized proteins is achieved. Clarifying the function of ECH could explain its role at the TGN and, importantly, help to unravel the complexity of the TGN's secretory pathways.

To better understand TGN function and the critical role of ECH, we performed a suppressor screen of the *ech* mutant phenotype. This revealed that a single amino acid substitution replacing glycine with glutamic acid at position 163 in the evolutionarily conserved protein TYPHON 1 (TPN1) creates a dominant suppressor mutation that restores the defects in hook formation and secretion caused by loss of ECH function. Additionally, this mutation relieves the ECH dependency of the TGN localization of the TPN1 protein. Furthermore, we demonstrate that the activity of the Golgi/TGN-localized small GTPase RABH1b is crucial for TPN1-mediated *ech* suppression, indicating that ECH acts via RAB-GTPase localization/function at the TGN.

Results

A single amino acid substitution in the TYPHON1 protein can suppress the phenotypic defects of the *ech* mutant

To identify the molecular components that act together with ECH to regulate differential growth and apical hook formation, an ethyl methanesulfonate (EMS) suppressor screen was performed on *ech* seeds. We used deep sequencing and comparative SHORE mapping (Schneeberger et al. 2009) of the F2 generation of twice backcrossed (BC2F2) plants of one such suppressor named TYPHON1 (TPN1, after Typhon, the consort of Echidna in Greek mythology). The causal mutation that suppressed the root, hypocotyl, and apical hook defects of *ech* in the TPN1 suppressor was found to be located within the gene At5g26740. Sequencing this locus in suppressed and nonsuppressed BC2F2 plants revealed that the causal EMS mutation is a Gly to Glu substitution at amino acid position 163 of the TPN1 protein. To verify that this substitution is indeed the causal mutation, we transformed *ech* plants with a construct expressing a mutated version of the *TPN1* gene with this substitution ($TPN1^{G163E}$) from the TPN1 promoter. Complete suppression of *ech* hook defects was observed both in the twice backcrossed homozygous F3 generation (BC2F3) of EMS-suppressed *ech* plants (referred to as ech^{supp}) and in 2 independent single insertion transformed lines (*ech*; $TPN1_{pro}$:$TPN1^{G163E}$ Line-1 and Line-2; see Fig. 1A). Both the ech^{supp} line and *ech*; $TPN1_{pro}$:$TPN1^{G163E}$ lines exhibited similar suppression of the primary root elongation (Supplementary Fig. S1A and B), hypocotyl elongation (Supplementary Fig. S1C and D), rosette growth (Supplementary Fig. S1E), flower bolt growth (Supplementary Fig. S1F), root hair formation (Supplementary Fig. S1G), and seed coat mucilage secretion (Supplementary Fig. S1H) defects of the *ech* mutant. In contrast, we could not observe any suppression of the *ech* phenotypic defects by transforming the WT version of *TPN1* ($TPN1_{pro}$:$TPN1^{WT}$) into the *ech* mutant background (Supplementary Fig. S2). These observations establish that the Gly^{163} to Glu substitution in TPN1 is the causal mutation of the phenotypic suppression in *ech* mutant.

Importantly, the *TPN1* gene has a close paralogue (At3g05940) whose encoded protein has 85% amino acid sequence identity and 93% sequence similarity with TPN1 (Supplementary Fig. S3A and B). We therefore named this second protein TYPHON2 (TPN2). The Gly^{163} residue that was mutated in TPN1 is conserved in TPN2. Therefore, we investigated whether changing this conserved residue in TPN2 (as in TPN1) could also suppress the *ech* phenotype. To this end, we engineered a construct expressing a $TPN2^{G163E}$ protein from the TPN1 promoter and expressed it in the *ech* mutant. *ech* plants transformed with the $TPN1_{pro}$:$TPN2^{G163E}$ construct showed suppression of *ech* hook defects like $TPN1^{G163E}$ lines (Supplementary Fig. S4). The $TPN1^{G163E}$ and $TPN2^{G163E}$ proteins are thus functionally interchangeable in terms of *ech* suppression. Altogether these results demonstrate that TPN1 and its close paralogue TPN2 act as novel genetic suppressors of the *ech* mutation when a conserved glycine residue is mutated to glutamic acid.

TPN1 restores defective AUX1 secretion and ethylene responsiveness in the *ech* mutant

ECH is required for secretion of the auxin transporter AUX1 from the TGN to the PM. Reduced PM levels of Yellow Fluorescent Protein-tagged AUX1 (AUX1-YFP) were therefore observed in an earlier study in the *ech* mutant (Boutté et al. 2013). In contrast with the parental *ech* mutant, PM levels of AUX1-YFP were restored to those seen in the WT in *ech*; $TPN1_{pro}$:$TPN1^{G163E}$ apical hooks (Fig. 1B and C). To confirm these results, we isolated microsomal membrane fraction from dark-grown whole seedlings expressing AUX1-YFP in WT, *ech* or *ech*; $TPN1_{pro}$: $TPN1^{G163E}$ backgrounds. While we detected a band of the expected size in WT, the intensity of that band strongly decreased in the *ech* mutant background and was completely rescued by TPN^{G163E} (Supplementary Fig. S5). In the *ech* mutant, we detected a degraded form of AUX1-YFP that is consistent with its vacuolar mislocalization in this genetic background (Boutté et al. 2013). AUX1 is required for the ethylene response leading to differential growth during apical hook development. Consequently, reduced levels of AUX1 cause ethylene insensitivity in the apical hook in the *ech* mutant; whereas apical hook exaggeration is seen in WT seedlings upon treatment with the ethylene precursor aminocyclopropane-1-carboxylate (ACC) (Fig. 1D; left, middle), this is not observed in ACC-treated *ech* seedlings. However, the WT-like behavior is observed in *ech*; $TPN1^{G163E}$ seedlings upon ACC treatment (Fig. 1D, right). These results indicate that TPN1 suppresses secretory defects in *ech*, leading to the restoration of AUX1 levels at the PM and the ethylene response in the apical hook.

TGN localization of $TPN1^{WT}$ but not $TPN1^{G163E}$ depends on ECH

The ECH protein localizes to the TGN, where it mediates secretion to the PM. Since the TPN1 mutation suppresses secretory defects in the *ech* mutant, we investigated the localization of the TPN1 protein by generating fluorescently tagged (Venus) versions of $TPN1^{WT}$ and $TPN1^{G163E}$ proteins expressed from the native TPN1 promoter and transformed these into WT plants. $TPN1^{WT}$-Venus localized to punctate structures in epidermal cells in the apical hook region. These $TPN1^{WT}$-Venus structures showed good overlap with TGN markers mCherry-Vesicle transport v-SNARE 12 (mCherry-VTI12) (Geldner et al. 2009) (colocalization frequency: 76.6%) and monomeric KusabiraOrange tagged Clathrin Light Chain (Ito et al. 2012) (mKO-CLC), for which the colocalization frequency was 51% (Fig. 2A to C). In contrast, the $TPN1^{WT}$-Venus signal exhibited only limited colocalization with the Golgi marker mCherry-SYNTAXIN OF PLANTS 32 (mCherry-SYP32); (Supplementary Fig. S6, colocalization frequency 21%). The localization of $TPN1^{G163E}$-Venus was similar, with 72% and 56% overlap with mCherry-VTI12 and mKO-CLC, respectively (Fig. 2D to F). These results indicate that TPN1, like ECH, localizes to the TGN and that the Gly^{163}Glu mutation in TPN1 that suppresses the *ech* phenotype does not alter its TGN localization. However, since

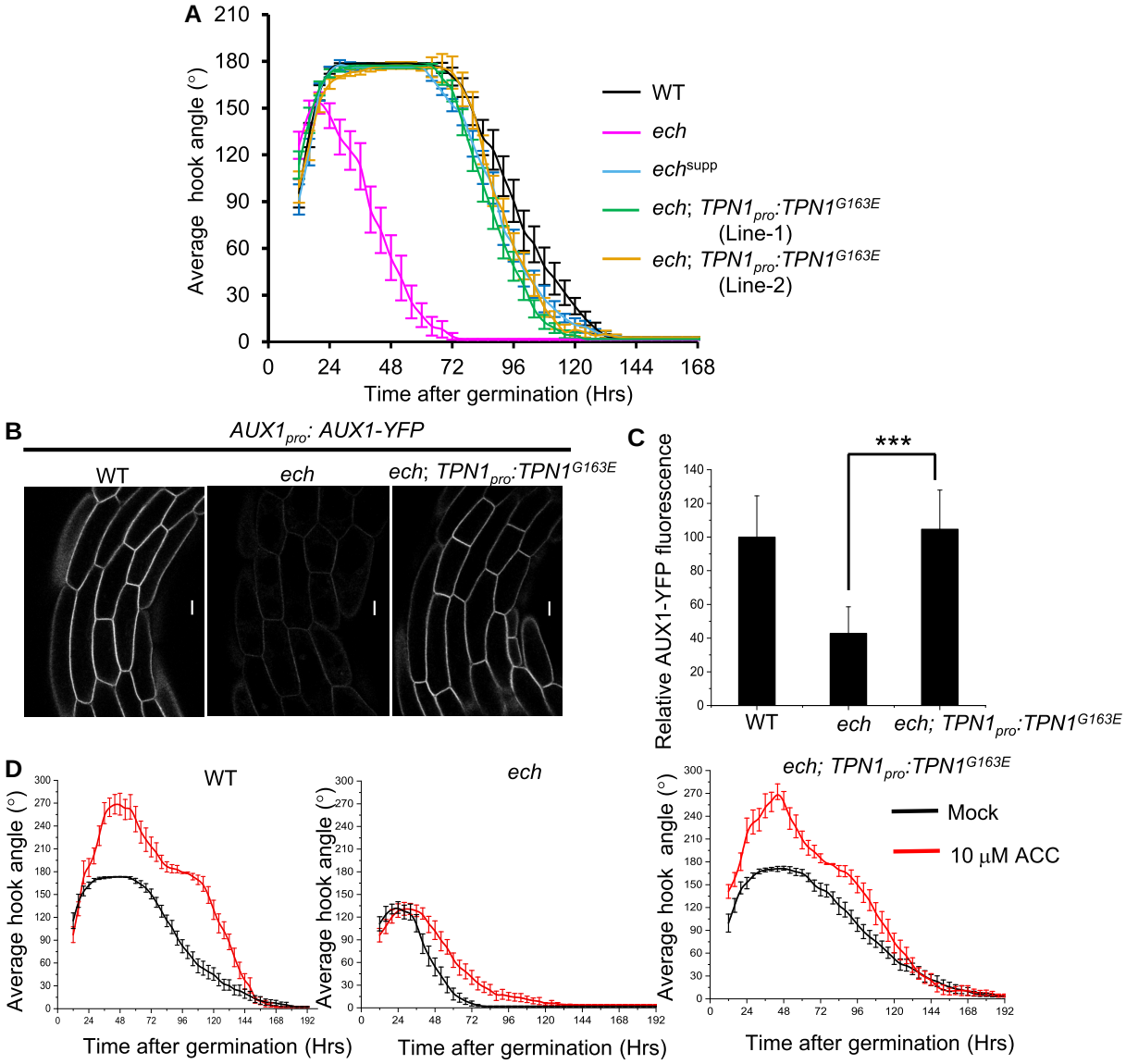

Figure 1. Point mutation in TPN1 gene suppresses hook defects of *ech* mutant. **A)** Time-lapse apical hook angle measurement in WT, *ech*, *ech*^{supp}, and *ech* transformed with TPN1^{G163E} construct (*ech; TPN1*$_{pro}$*:TPN1*^{G163E}, 2 independent lines), $n = 20$ seedlings/group. **B)** and **C)** Representative image **(B)** and quantification **(C)** of AUX1-YFP signal in the apical hook region of WT, *ech* and *ech; TPN1*$_{pro}$*:TPN1*^{G163E} seedlings. $n = 50$ cells from 5 seedlings. **D)** Apical hook exaggeration in WT hooks treated with 10 μM ACC, (left) is abrogated in *ech* (middle) but is restored in *ech; TPN1*$_{pro}$*:TPN1*^{G163E}seedlings (right) $n = 20$ seedlings/group. In **A** and **D**, error bars represent standard error of the mean. In **C**, error bars represent standard deviation. ***$P < 0.001$ (*t*-test). Scale bar 10 μm.

TPN1 suppresses the *ech* mutant phenotype, we investigated the ECH dependence of TPN1 localization to TGN. In contrast to their very similar localization in WT seedlings, the localization of TPN1^{WT}-Venus and TPN1^{G163E}-Venus differed markedly in the *ech* background. In *ech*, TPN1^{WT}-Venus was partially mislocalized in larger membranous structures that were stained by acidic vacuolar marker dye Lysotracker Red (Fig. 2G and Supplementary Fig. S7, arrows). The mislocalization of TPN1 from the TGN to the vacuoles is highly reminiscent of the previously reported mislocalization of various TGN-resident proteins in *ech* (Gendre et al. 2011).

In contrast, TPN1^{G163E}-Venus maintained its punctate localization in *ech* (Fig. 2G). We confirmed that TPN1^{G163E}-Venus localizes to TGN in *ech* by monitoring its colocalization with the CHC, which localizes to the TGN in an ECH-independent manner (Supplementary Fig. S8). This indicates that the localization of TPN1^{WT} depends on ECH and that the single amino acid change from TPN1 to TPN1^{G163E} is sufficient to restore localization of TPN1^{G163E} to punctate TGN structures even in the absence of ECH. TPN1^{G163E} thus restores both AUX1 levels at the PM and ethylene sensitivity while it suppresses the hook defects of *ech* (Fig. 2H). These results strongly support the hypothesis that the suppression of the *ech* phenotype caused by a single amino acid change in TPN1 is due to restoration of the latter protein's TGN localization.

tpn mutants display genetic interaction with *ech*

To determine the molecular functions of TPN proteins, we studied loss of function T-DNA insertion mutants of TPN1 and the closely related TPN2 using homozygous *tpn1* and *tnp2* mutants (Supplementary Fig. S9A to D) that lacked full-length *TPN1* and *TPN2* mRNAs, respectively (Supplementary Fig. S9E). We found that these mutants lacked apical hook defects (Fig. 3A). To rule out

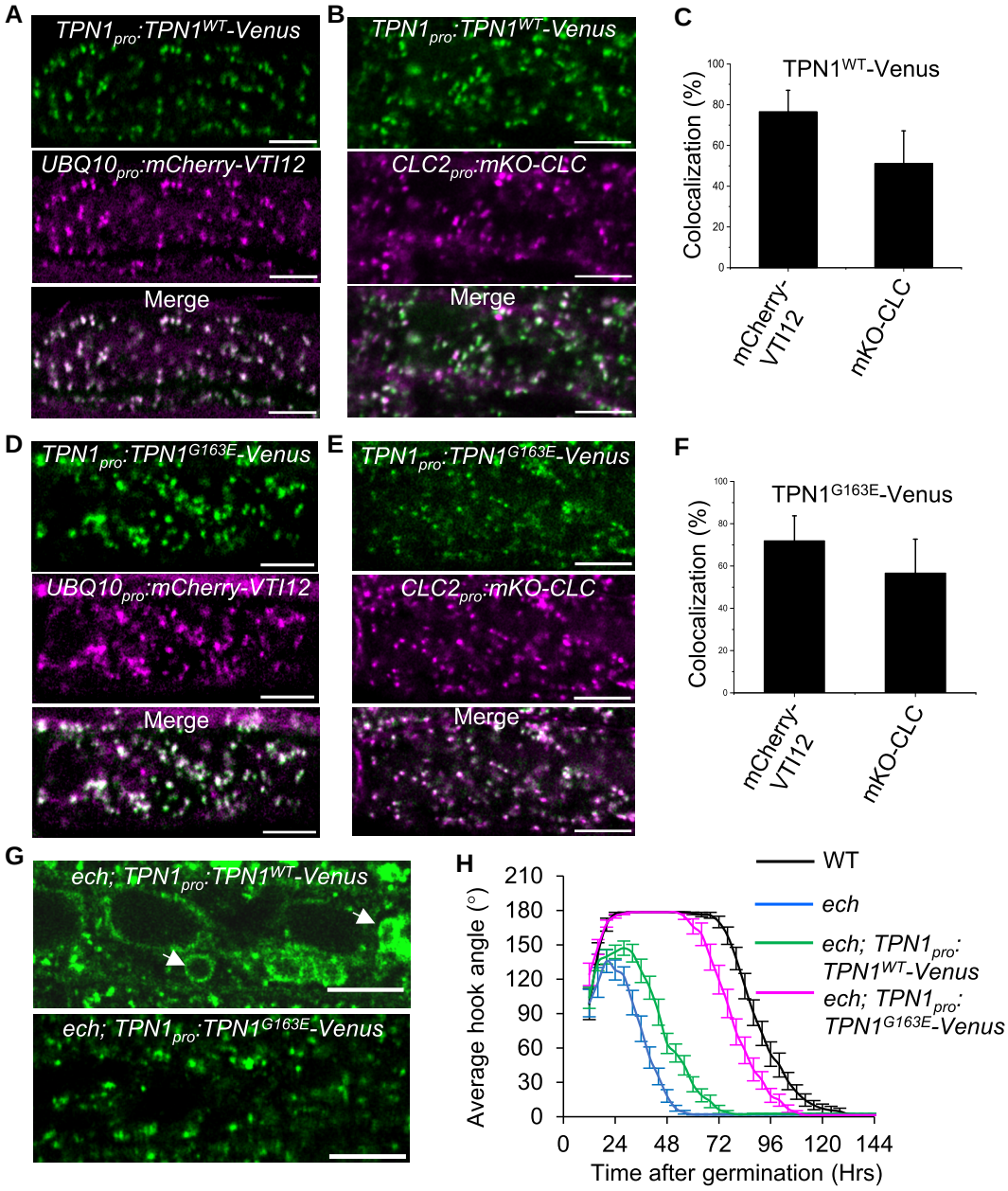

Figure 2. TPN1 is a TGN-localized protein. **A)** and **B)** Colocalization of TPN1^{WT}-Venus with TGN-localized SNARE mCherry-VTI12 **(A)** and mKO-CLC **(B)** in epidermal cells of apical hook region. Quantification of colocalization is shown in **C**. **D)** and **E)** Colocalization of TPN1^{G163E}-Venus with mCherry-VTI12 **(D)** and mKO-CLC **(E)**. Quantification of colocalization is plotted in **F**. $n \geq 20$ cells from 5 seedlings for **C** and **F**, error bars represent standard deviation. **G)** Localization of TPN1^{WT}-Venus and TPN1^{G163E}-Venus in epidermal cells of hook region of *ech* mutant. TPN1^{WT}-Venus is localized to larger, vacuole-like structures in *ech* mutant (arrows) while TPN1^{G163E}-Venus maintains punctate localization. **H)** Time-lapse apical hook angle measurement in WT, *ech*, *ech*; *TPN1^{WT}-Venus* and *ech*; *TPN1^{G163E}-Venus* seedlings ($n \geq 16$ seedlings/group). Error bars represent the standard error of the mean. Scale bar: 10 μm.

possible functional redundancy, we generated a *tpn1 tpn2* double mutant by crossing the single mutants. However, the *tpn1 tpn2* mutant also had no significant hook defects (Fig. 3A). We therefore used an alternate approach to investigate genetic links between ECH and TPN activity. Although the single *tpn1* mutant had no apical hook phenotype, introducing *tpn1* or *tpn2* into *ech* to form *ech tpn1* and *ech tpn2* double mutants significantly enhanced the hook defects of the single *ech* mutant (Fig. 3B). Additionally, *tpn1* and *tpn2* mutants exacerbated the root growth defects of light-grown seedlings when combined with *ech* (Supplementary Fig. S10A and B) as well as the stature of soil-grown *ech* plants (Supplementary Fig. S10C). Moreover, *ech tpn2 tpn1*$^{+/-}$ plants had a severely stunted phenotype (Supplementary Fig. S10C) and produced no seeds. These results suggest a genetic relationship between *ech* and *tpn1* or *tpn2*. The colocalization of TPN1 and ECH proteins, the dependence of TPN1 on ECH for TGN localization, and the enhancement of the *ech* phenotype by single *tpn1* or *tpn2* mutants strongly suggest that the TPN proteins mediate the ECH pathway at the TGN.

RABH1b is essential for TPN1^{G163E}-mediated suppression of *ech* phenotypes

ECH interacts with the YIP4A/YIP4B proteins to form a complex that mediates secretion at the TGN (Gendre et al. 2013; McFarlane et al.

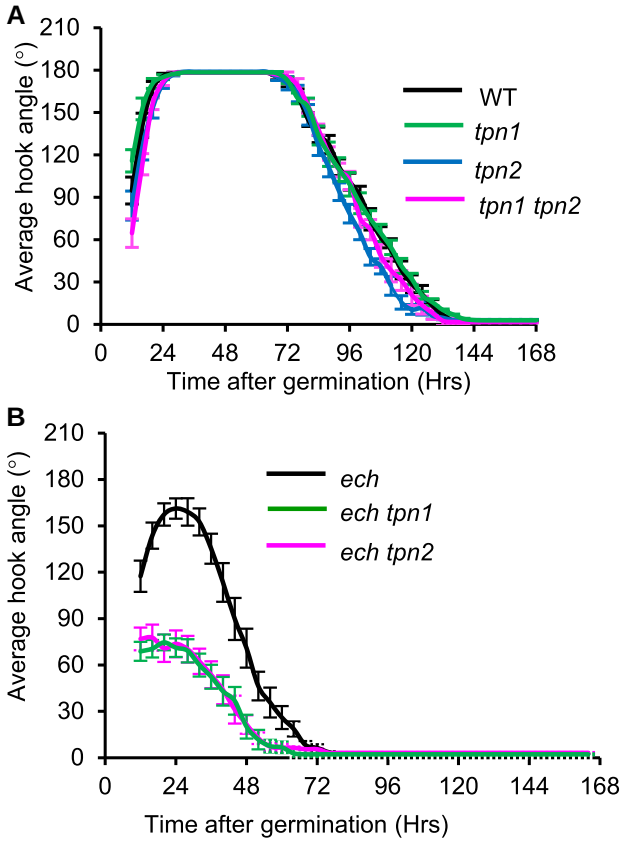

Figure 3. *tpn1* and *tpn2* genetically interact with *ech* for regulating apical hook formation. **A)** Time-lapse apical hook angle measurements in WT, *tpn1*, *tpn2*, and *tpn1 tpn2* mutant. **B)** Apical hook measurement in *ech* and *ech tpn1* or *ech tpn2* double mutants. $n \geq 16$ seedlings. Error bars represent standard error of the mean.

2013). The Golgi/TGN-localized RAB-GTPase RABH1b (AtRAB6) was recently identified as a downstream interactor of YIP4A/YIP4B proteins (Renna et al. 2018). Importantly, we found that a *rabh1b* loss of function mutant had an apical hook defect (Supplementary Fig. S11A). Single mutant of the other members of the RABH class did not show any hook phenotype (Supplementary Fig. S11A) indicating that despite the redundancy, RABH1b has a pivotal role during the early seedling development of apical hook. Additionally, like *ech*, the *rabh1b* mutant was ethylene-insensitive (Supplementary Fig. S11B) and exhibited reduced PM levels of AUX-YFP relative to the WT (Supplementary Fig. S11C and D). Also, the localization of RABH1b was dependent on ECH because the punctate localization of GFP-tagged RABH1b (GFP-RABH1b) in the apical hook region epidermal cells of *ech* was markedly lower than in the WT (Fig. 4A and B). In contrast, other TGN-localized RAB-GTPases (RABA5d, RABA1e, and RABE1d) were not mislocalized in *ech* (Supplementary Fig. S12). These results prompted us to investigate whether the *ech* suppression by TPN1^{G163E} involves RABH1b. Interestingly, we found that in contrast with the mislocalization of RABH1b in the *ech* mutant (Fig. 4A and B), the punctate localization of GFP-RABH1b was restored to WT levels in *ech;* TPN1^{G163E} seedlings (Fig. 4A and B).

This restoration of GFP-RABH1b localization by TPN1^{G163E} prompted us to investigate the possible interaction between RABH1b and TPN1 through bimolecular fluorescence complementation (BiFC) assay. Coexpression of TPN1^{WT} or TPN1^{G163E} fused with the N terminus of yellow fluorescent protein (nYFP) and RABH1b fused to the C terminus of yellow fluorescent protein (cYFP) in Arabidopsis protoplasts displayed YFP fluorescence in punctate structures (Supplementary Fig. S13A and B, arrows) which were distinct from the cytosolic red fluorescence protein (RFP) signal that served as transfection control. Under similar acquisition settings, we did not detect any YFP fluorescence in RFP-expressing protoplasts transfected with a construct expressing only nYFP + cYFP or nYFP + cYFP fused with RABH1b (Supplementary Fig. S13C and D). Quantification of fluorescence intensities revealed a significantly higher YFP/RFP fluorescence ratio in protoplasts expressing TPN1^{WT}–nYFP + cYFP-RABH1b and TPN1^{G163E}–nYFP + cYFP-RABH1b compared to protoplasts expressing nYFP + cYFP-RABH1b or nYFP + cYFP (Supplementary Fig. S13E). Additionally, we expressed *TPN1$_{pro}$:TPN1*^{WT}-mCherry or *TPN1$_{pro}$:TPN1*^{G163E}-mCherry construct together with *RABH1b$_{pro:}$ GFP-RABH1b* in Arabidopsis protoplasts and found TPN1^{WT}-mCherry and TPN1^{G163E}-mCherry labeled punctate structures overlapped with GFP-RABH1b structures in dual transfected protoplasts (Supplementary Fig. S14A and B) with similar colocalization frequencies (Supplementary Fig. S14C). To further assess the proximity between RABH1b and TPN1 as suggested by BiFC results, we measured the average fluorescence lifetime of GFP (Rios et al. 2017) in protoplasts expressing only GFP-RABH1b or GFP-RABH1b together with mCherry-tagged TPN1. There was a significant reduction in GFP lifetime in the presence of TPN1^{WT}-mCherry or TPN1^{G163E}-mCherry compared to GFP-RABH1b alone (Supplementary Fig. S14D). Such reduction of fluorescence lifetime is indicative of Förster resonance energy transfer between GFP and mCherry fluorophores suggesting close physical proximity and presumable interaction between RABH1b and TPN1^{WT} or TPN1^{G163E}. To further explore the involvement of RABH1b in TPN1^{G163E}-mediated *ech* suppression, we introduced the *rabh1b* mutation in the *ech;* TPN1^{G163E} background. Loss of RABH1b completely eliminated the ability of TPN1^{G163E} to suppress the phenotypic defects of *ech* (Fig. 4C and D and Supplementary Fig. S15). The resulting *ech rabh1b;* TPN1^{G163E} triple mutant seedlings displayed hook defects that were identical to those of *ech* seedings and somewhat more pronounced than the defects of *rabh1b* (Fig. 4C). Similarly, the root length of light-grown *ech rabh1b;* TPN1^{G163E} triple mutant seedlings and the hypocotyl length of their dark-grown counterparts were more like those of *ech* than the *ech;* TPN1^{G163E} double mutant (Supplementary Fig. S15A to D). Consistently, 3- and 6-wk-old soil-grown *ech rabh1b; TPN1$_{pro}$:TPN1*^{G163E} plants exhibited stunted growth like *ech* (Fig. 4D). Finally, the apical hook phenotype of the *rabh1b tpn1 tpn2* triple mutant is identical to the *rabh1b* single mutant (Supplementary Fig. S16A). Importantly, the localization of *TPN1$_{pro}$:TPN1*^{WT}*-Venus* or *TPN1$_{pro}$:TPN1*^{G163E}*-Venus* remains unaltered in *rabh1b* (Supplementary Fig. S16B and C), which implies that the proper localization of TPN, upon native expression, is directly dependent on ECH rather than downstream RABH1b activity. Together with the failure of TPN1^{G163E}-Venus to suppress the hook phenotype of the *rabh1b* mutant (Supplementary Fig. S16D), these results suggest that the ECH/TPN1 module influences RABH1b localization and that RABH1b acts downstream of the ECH/TPN1 module in the TGN.

Discussion

The plant TGN is the hub where secretion, vacuolar transport, endocytosis, and recycling pathways intersect (Gendre et al. 2015). How the TGN regulates and balances these distinct processes remains unclear (Rosquete et al. 2018; Renna and Brandizzi 2020). Recent studies have revealed distinct subdomains within the TGN that are involved in vesicular trafficking to the PM or the vacuole (Fuji et al. 2016; Shimizu et al. 2021). Additionally, it has been established that unique regulators govern the secretion of

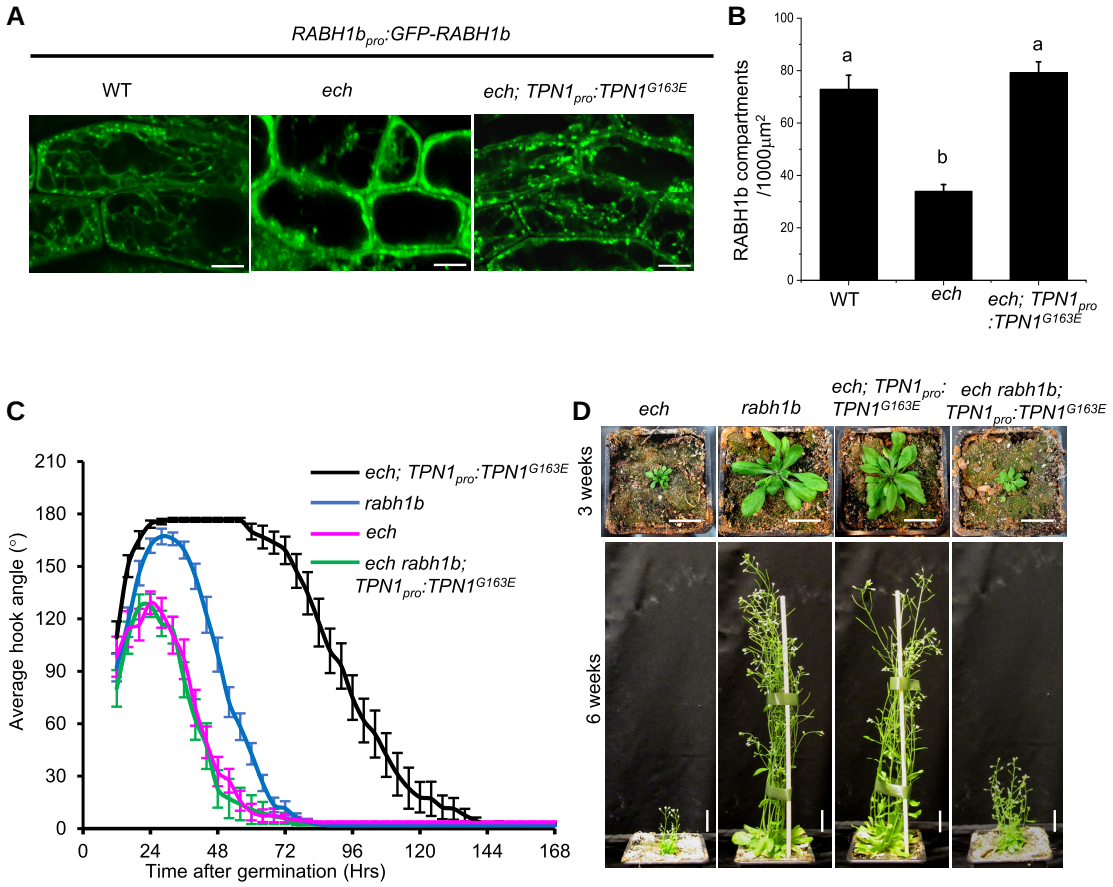

Figure 4. RABH1b is required for *ech* suppression by TPN1^{G163E}. **A)** Localization of GFP-RABH1b in epidermal cells in apical hook regions of dark-grown WT, *ech* and *ech*; *TPN1$_{pro}$:TPN1^{G163E}*seedlings. **B)** Quantification of number of GFP-RABH1b compartments in WT, *ech* and *ech; TPN1$_{pro}$:TPN1^{G163E}* seedlings, $n \geq 20$ cells from 5 seedlings. Error bars represents standard deviation. Groups with a significant difference by one-way ANOVA with post hoc Tukey's test ($P < 0.001$) are indicated by different letters. **C)** Time-lapse quantification of apical hook angles in dark-grown *ech*, *rabh1b*, *ech; TPN1$_{pro}$:TPN1^{G163E}*and *ech rabh1b; TPN1$_{pro}$:TPN1^{G163E}*seedlings. ($n = 16$ seedlings/group). Error bars represent standard error of the mean. **D)** 3- and 6-wk-old *ech*, *rabh1b*, *ech TPN1$_{pro}$:TPN1^{G163E}*and *ech rabh1b; TPN1$_{pro}$:TPN1^{G163E}*plants. Scale bar: 10 μm for **A** and 2 cm for **D**.

specific cargoes by the systems responsible for TGN to PM trafficking. For example, the loss of TGN-localized ENTH proteins inhibited the secretion of seed coat mucilage without affecting the apoplastic secretion of a fluorescent reporter protein (Heinze et al. 2020). Complementarily to proteins, the lipid composition of membranes is an essential regulator of protein sorting at TGN. The acyl-chain length of sphingolipids is involved in the sorting of PIN2 at TGN through a mechanism that consumes the anionic lipid phosphatidylinositol-4-phosphate (PI4P) (Wattelet-Boyer et al. 2016; Ito et al. 2021). Interestingly, while this sphingolipid/PI4P coupling mechanism targets the secretion of the auxin transporter PIN2 but not that of PIN1, PIN7, or AUX1, loss of ECH specifically affected secretion of AUX1 but not of PIN2, PIN3, or LAX3 (Gendre et al. 2011; Boutté et al. 2013; Wattelet-Boyer et al. 2016), and loss of *ech* function caused mislocalization of a subset of key TGN-resident trafficking regulators (Gendre et al. 2011; Jonsson et al. 2017). The observation of specific defects in AUX1 secretion together with normal secretion of PINs to the PM could be due to dysregulation of a subset of TGN-localized proteins. In accordance with this hypothesis, the *ech* suppressor identified in this work, TPN, displayed an ECH-dependent localization pattern. Single and double *tpn* mutants have no detectable phenotype, which makes the suppression of severe secretory and growth defects in *ech* by a single amino acid change in TPN intriguing. TPN^{G163E} is a dominant suppressor mutation, and importantly, this mutation results in retention of TPN^{G163E} at TGN even in the absence of ECH. The fact that TPN^{G163E} remains at TGN in the *ech* mutant rather than being mislocalized like TPN^{WT} shows that in the absence of ECH, TPN is able to restore a functional TGN-secretion. Despite this, there is strong evidence that ECH and TPNs act in a common pathway based on the TGN localization of TPN1, its mislocalization in *ech*, and the genetic interaction of TPNs with ECH that causes mutations in either *tpn1* or *tpn2* to massively enhance the *ech* phenotype. Thus, these results suggest that TPNs more likely to act as facilitators of ECH function rather than directly being essential executors of ECH function.

TPN1 belongs to the evolutionarily conserved transmembrane organic solute transporter alpha (OSTA) family. OSTA-1, the homolog of TPN1 in *Caenorhabditis elegans*, localizes to endocytic and secretory compartments and regulates the dynamics of RAB5 GTPases (Olivier-Mason et al. 2013). Interestingly, our biochemical and genetic studies identified the YIPs YIP4a and YIP4b as interactors of ECH (McFarlane et al. 2013). YIP proteins are reported to interact with and regulate the activity of RAB-GTPases in yeast and mammalian systems (Sivars et al. 2003; Kranjc et al. 2017). RAB-GTPases perform diverse secretory functions in processes including vesicle budding and transport, docking, tethering, and fusion with the destination membrane (Zheng et al. 2015; Pfeffer 2017). The secretory defects of *ech* and *yip4a yip4b* mutants may therefore stem from mislocalization/dysregulation of downstream RAB-GTPases. Several RAB-GTPases belonging to the clades RABA,

RABB, RABD, RABE, RABG, and RABH localize to the TGN (Chow et al. 2008; Drakakaki et al. 2012; Qi and Zheng 2013). Amongst these, RABH1b has been demonstrated to interact with YIP4 proteins (Renna et al. 2018) and therefore is a likely molecular effector acting downstream of YIP4 and ECH. In support of this hypothesis, we found that the number of GFP-RABH1b-labelled compartments is dramatically reduced in the *ech* mutant. We previously found that the localization of RAB-GTPase RABA2a was not altered in *ech* (Gendre et al. 2011). Additionally, we showed that the Golgi/TGN localization of YFP-RABA1e (Asaoka et al. 2013), RFP-RABE1d (Speth et al. 2009), and mCherry-RABA5d (Geldner et al. 2009) were unchanged in *ech*. These results suggest that ECH interacts specifically with RABH1b rather than the multitude of other Golgi/TGN-localized RAB-GTPases. RABH1b has been shown to mediate the secretion of cellulose synthase complex 6 and to regulate the hypocotyl length of dark-grown seedlings (He et al. 2018). However, the effects of the *rabh1b* mutant on differential growth and apical hook formation have not been explored. We found the *rabh1b* mutant has ethylene-insensitive hook formation defects and reduced PM levels of AUX1 like the *ech* mutant.

Although TPN1^{G163E} restored the punctate localization of GFP-RABH1b in *ech*, our BiFC and fluorescence lifetime measurement observations indicate that the putative interaction with RABH1b is not a unique feature of TPN1^{G163E}, since TPN1^{WT} protein interacts with RABH1b as well. Therefore, restoration of RABH1b localization in *ech* by TPN1^{G163E} possibly stems from the ability of this mutated version of TPN1 to retain its TGN localization in the absence of ECH, unlike the TPN1^{WT} protein.

The finding that loss of RABH1b eliminated TPN1^{G163E}-mediated suppression of *ech*, suggests that RABH1b plays a key role downstream of ECH/TPN module. This hypothesis is further supported by the observation that unlike the *ech* mutant, TPN1 ^{G163E} fails to suppress the apical hook formation defects of the *rabh1b* mutant. Moreover, the hook phenotype of the *rabh1b tpn1 tpn2* triple mutant is identical to the single *rabh1b* mutant, further supporting that RABH1b acts downstream of TPN. While the phenotypic defects of the *rabh1b* mutant are less severe than those of *ech*, this effect could be due to potential functional redundancy between the five members of the RABH clade (Vernoud et al. 2003). In the RABH clade, RABH1b is however the most prominently active member as single mutants of other members of the RABH clade do not display an apical hook defect. Given that RABH1b has been shown previously to be an effector of ECH-interacting proteins YIPs (Renna et al. 2018), we do believe that TPN is a new actor in the ECH/YIP/RABH secretory regulatory module at TGN.

In summary, we identified a module involving the proteins TPN1 and TPN2 that acts in ECH-mediated secretion at the TGN. Further investigations will be needed to determine how and why a single amino acid change enables the mutant TPN1 protein to be retained at the TGN in an ECH-independent manner unlike the WT TPN1 protein, but this mutation presumably suppresses *ech* defects by ensuring that other important secretory proteins such as RABH1b are retained at TGN and thereby restoring secretion. Recent advances in live super-resolution microscopy have provided unique insights into plant TGN organization. It is proposed that a TGN domain marked by the SNARE VESICLE-ASSOCIATED MEMBRANE PROTEIN 721 (VAMP721), the adapter AP1, and clathrin regulates TGN to PM transport while another domain marked by the SNARE VAMP727 and adapter AP4 regulate TGN to vacuole cargo transport (Shimizu et al. 2021). Interestingly, previous studies have found that a domain within the TGN marked by the SNARE SYP61 is also involved in TGN to PM transport (Boutté et al. 2013; Wattelet-Boyer et al. 2016). Proteomic characterization of immunopurified SYP61 vesicles identified both ECH and RABH1b as part of this domain of TGN (Drakakaki et al. 2012) and the loss of ECH specifically affected this domain of the TGN but not the domain containing clathrin-coated vesicles (Boutté et al. 2013). These results suggest a high complexity in TGN subdomain delineation. The specificity of ECH in regulating TGN to PM transport provides an essential molecular handle to dissect the dynamic interrelation of specialized TGN subdomains. Our results provide new insights into the complexity of the TGN's secretory functions and reveal previously uncharacterized components acting in the ECH pathway. A future survey of candidate protein localization and functionality in the single *ech* mutant and the double *ech*; TPN1^{G163E} mutant will shed further light on the organization of the unique ECH-dependent secretory machinery of the TGN.

Materials and methods

Plant materials and growth condition

The following *A. thaliana* mutant and transgenic lines have been described previously: *ech* (Gendre et al. 2011), *UBQ10$_{pro}$:mCherry-VTI12*, *UBQ10$_{pro}$:mCherry-RABA5D* and *UBQ10$_{pro}$:mCherry-SYP32* (Geldner et al. 2009), *CLC2$_{pro}$:mKO-CLC* (Ito et al. 2012), *35S$_{pro}$: YFP-MEMBRIN12* (Zhang et al. 2011), *RABA1e$_{pro}$:YFP-RABA1e* (Asaoka et al. 2013), *35S$_{pro}$:GFP-RABE1d* (Speth et al. 2009), *AUX1$_{pro}$:AUX1-YFP* (Swarup et al. 2004). Ecotype Col-0 was used as WT control in all experiments.

To identify knockout mutants of TPN1 and TPN2, we ordered all available T-DNA insertion mutants from the Nottingham Arabidopsis Stock Centre, UK. However, we detected t-DNA insertion only in one line each for TPN1 and TPN2. Homozygous *tpn1* (GABI_299D08) and *tnp2* (GABI_010G07) mutants were genotyped using the primers listed in Supplementary Table S1. The knockout mutants of RABH1a (GABI_461_D10), RABH1b (SAIL_91_H10), RABH1c (WiscDsLox451C07), RABH1d (SALK_134578), and RABH1e (SALK_119886) were obtained from the Arabidopsis Biological Resource Centre, USA. GoTaq DNA Polymerase (Promega) was used for PCR genotyping.

Plants were grown on soil in walk-in chambers under 16/8 h light/dark (150 μmol/m^2 light intensity) and 22 °C/18 °C temperature regimes. For apical hook experiments, seeds were sterilized for 5 min in 90% (v/v) ethanol + 10% (v/v) bleach, washed with 95% (v/v) ethanol for 2 min, and dried before sowing on the surface of agar plates (one-half Murashige and Skoog medium, pH 5.8, 1% [w/v] sucrose, 2.5 mM morpholinoethanesulfonic acid, 1% [w/v] plant agar, Duchefa Biochemie). After 3 d of stratification at 4 °C and 6 h light exposure to induce germination, seedlings were grown on vertical plates in the dark at 21 °C. For confocal microscopy, seedlings were imaged 24 h post germination. Light-grown plants were grown vertically under 16/8 h light/dark for the indicated durations. For membrane extraction experiments, seedlings were grown in the dark in liquid one-half Murashige and Skoog medium with 1% (w/v) sucrose and 2.5 mM morpholinoethanesulfonic acid (pH 5.8) for 7 d.

Time-lapse analysis of apical hook development

Seedlings were grown vertically on plates in a dark room at 21 °C. Seedlings were photographed at 4 h intervals using a Canon D50 camera without an infrared filter under illumination by an infrared light-emitting diode light source (850 nm). Captured images were opened as sequences in Fiji/ImageJ, and apical hook was measured using the angle measurement tool. Conventionally, fully closed and fully open hooks are considered to have angles of 180° and 0°, respectively (Boutté et al. 2013). Thus, the values

of 180° measured hook angle were plotted against time to generate kinematics graphs of apical hook development. At least 16 plants were measured/grouped. Error bars in the graphs represent the standard error of mean.

EMS seed mutagenesis

About 10,000 *ech* VHAa1-GFP seeds (180 mg) were soaked overnight in distilled water before adding EMS at a final concentration of 0.3% (v/v). After 11 h of incubation on a rotator, the seeds were washed 6 times with water, suspended in 0.1% (w/v) agar, and stored for 3 d at 4 °C before being sown (~12 seeds/pot). Plants were harvested in batches of 25 individuals (M1).

Suppressor mutant screening

600 seeds from each M1 batch were screened for hypocotyl length and seedlings with an increased hypocotyl length compared to *ech* were selected. Subsequently, all dark-grown seedlings were transferred to light for 3 d and screened for root hair restoration. Seedlings showing improved hypocotyl growth and root hair density were transferred to the soil. Seeds were individually harvested from each plant (M2). Seedlings germinated from M2 seeds were further screened for improved hypocotyl growth, hook formation, improved root growth, and root hair restoration. These seedlings were transferred to soil to produce M3 seeds. After screening the progenies of M3 seeds, a suppressor line exhibiting consistent improvement relative to the *ech* phenotype was chosen for further analysis. This line was backcrossed twice with the parental *ech* VHAa1-GFP line to reduce background mutations before sequencing.

SHORE mapping and mutation identification

We used mapping-by-sequencing/SHORE mapping (Schneeberger et al. 2009) of BC2F2 plants to find the causal mutation in the EMS-suppressed *ech* line. 800 BC2F2 seeds were sown on MS plates and after 7 d growth, 400 WT-like seedlings were transferred onto soil together with 100 *ech*-like seedlings. Rosette leaves from these plants were harvested and flash-frozen. Leaf materials from plants that produced homozygous WT-like progeny were used for nuclear DNA extraction as described previously (Lutz et al. 2011). Nuclear DNA extracted from rosette leaves of *ech*-like BC2F2 plants was used as a sequencing control to eliminate background mutations. DNA concentrations were determined using a NanoDrop 2000c UV–Vis spectrophotometer (Thermo Fisher). 5 μg of freeze–dried DNA per sample was sent to IGA Technologies (Uden, Italy) for Illumina sequencing. Sequencing results were analyzed using the SHOREmap software package (https://1001genomes.org/software/shoremap.html), revealing the TPN1^{G163E} mutation (G488A substitution in At5g26740 ORF).

cDNA synthesis and reverse transcription-PCR

mRNA was extracted from 7-d-old light-grown seedlings using the Spectrum Plant Total RNA Kit (Sigma-Aldrich). Following genomic DNA removal using the DNA-free DNA Removal Kit (Thermo Fisher), the mRNA was converted to cDNA using the SuperScript IV First-Strand Synthesis System (Thermo Fisher). Expression of TPN1, TPN2, and Tublin Alpha 3 (TUA3) was verified using the indicated primers (Supplementary Table S1) and Phusion DNA Polymerase (Thermo Fisher).

Cloning and generating transgenic lines

For cloning *TPN1$_{pro}$:TPN1*^{WT}/*TPN1*^{G163E} constructs, the 1.8-kb promoter region of TPN1 gene was amplified from Col-0 genomic DNA using the primers TPN1 promoter FWD (*Bam*HI) and TPN1 promoter REV (*Asc*I). Separately, a 2.3-kb genomic DNA fragment containing the TPN1 gene was amplified using the primers TPN1 5′ UTR-FWD/1F and TPN1 3′ UTR-REV/1R from either Col-0 genomic DNA (For TPN1^{WT}) or homozygous *ech*^{supp} plants (for TPN1^{G163E}). The TPN1 coding region (from start to stop codon) was amplified using primers TPN1 FWD (PacI) and TPN1 REV (SpeI). The TPN1 promoter was cloned in the *Bam*HI and AscI digested plasmid pSL34 (Ikeda et al. 2009) to generate plasmid pSL34-*TPN1$_{pro}$*. The resulting plasmid was digested with PacI and SpeI to ligate the TPN1^{WT} or TPN1^{G163E} coding region to generate the constructs pSL34-*TPN1$_{pro}$:TPN1*^{WT} or pSL34-*TPN1$_{pro}$:TPN1*^{G163E}. For Venus/mCherry-tagged versions of TPN1, TPN1^{WT}, or TPN1^{G163E}, coding regions were amplified without a stop codon using the primer TPN1 FWD (PacI) + TPN1 no stop REV (SpeI) and cloned upstream of the Venus/mCherry coding sequence of pSL34-Venus or pSL34-mCherry (Ikeda et al. 2009) using *Pac*I and *Spe*I digestion. The *TPN1$_{pro}$:TPN1-Venus/mCherry* cassettes were transferred from pSL34 to pGreenII0179 using *Bam*HI and *Not*I.

To clone the *TPN1$_{pro}$:TPN2*^{G163E} construct, a 2.1-kb genomic DNA fragment containing the TPN2 gene was amplified using the primers TPN2 5′ UTR-FWD/2F and TPN2 3′ UTR-REV/2R from Col-0 genomic DNA. To introduce the G^{163}E point mutation, 2 separate fragments were amplified using the primer pairs TPN2 FWD (AscI) + TPN2 SDM REV and TPN2 SDM FWD + TPN2 REV (*Not*I). The fragments were fused by PCR and cloned in the plasmid pSL34-*TPN1$_{pro}$* (described above) by *Asc*I and *Not*I digestion. FastDigest restriction enzymes and T4 DNA ligase (Thermo Fisher) were used for the cloning.

For *RABH1b$_{pro}$:GFP-RABh1b*, the relevant genomic fragment (1.0 kb of the 5′-flanking sequence and 1.1 kb of the 3′-flanking sequence of RABH1b) was amplified using primers RABH1b genomic-FWD and RABH1b genomic-REV and subcloned into the pENTER^{TM}/D-TOPO^{TM} entry vector (Thermo Fisher Scientific). The cDNA encoding GFP was inserted in front of the start codon of RABH1B using the In-Fusion HD Cloning Kit (Clontech), and then recombined into the destination vector pHGW (Karimi et al. 2002) using the Gateway LR Clonase-II enzyme mix (Thermo Fisher Scientific).

For cloning BiFC constructs, genomic sequences of TPN1^{WT} or TPN1^{G163E} without the stop codon were amplified from the plasmids pSL34-*TPN1$_{pro}$:TPN1*^{WT} or pSL34-*TPN1$_{pro}$:TPN1*^{G163E} respectively, using primers TPN1-attB3-FWD + TPN1-attB2-REV. The resulting amplicons were cloned in the plasmid pDONR221-P3P2 (Thermo Fisher) using Gateway^{TM} BP clonase-II enzyme mix (Thermo Fisher). RABH1b genomic sequence (with stop codon) was cloned from the plasmid pHGW-*RABH1b$_{pro}$:GFP-RABh1b* using primers RABH1-attB1-FWD + RABH1-attB4-REV and the amplicon was cloned in the plasmid pDONR221-P1P4 (Thermo Fisher) using BP clonase-II enzyme. The pDONR221 plasmids containing RABH1b and TPN1^{WT}/TPN1^{G163E} were combined in pBiFCt-2 in 1-CN plasmid (Grefen and Blatt 2012) using LR Clonase-II Plus Enzyme Mix (Thermo Fisher). In the final construct N-terminal half of YFP (nYFP) was cloned *in-frame* downstream to TPN1^{WT}/TPN1^{G163E} and C-terminal half of YFP (cYFP) was cloned *in-frame* upstream to RABH1b. The vector contains separate cassette coding RFP, which can be used to identify transfected protoplasts. RABH1b was cloned alone in pBiFCt-2 in 1-CN to be used as a negative control.

The binary vectors were introduced into *Agrobacterium tumefaciens* strain GV3101-pMP90-pSoup by electroporation. Arabidopsis Col-0 plants were transformed using the floral dip method (Clough and Bent 1998). The presence of the TPN1^{G163E}/TPN2^{G163E} mutations was verified by PCR using derived cleaved-amplified polymorphic sequence (dCAPS) primers (http://helix.wustl.edu/dcaps/dcaps.html) followed by *Pdm*I digestion. All cloning and genotyping primers are listed in Supplementary Table S1.

Protoplast transfection

Protoplasts were generated from Arabidopsis suspension cell culture (Fülöp et al. 2005) and transfected following previously published methods (Mathur and Koncz 1998). Briefly, 4-d-old suspension-cultured cells were digested with 1% (w/v) cellulase (Onozuka R-10, Serva catalogue no: 16419) and 0.2% (w/v) macerozyme (Onozuka R-10, Serva catalogue no: 28302) dissolved in Gamborgs B5 medium pH 5.8, supplemented with 340 mM glucose + 340 mM mannitol for 4 h in dark to generate protoplasts. Protoplasts were enriched by flotation on Gamborg's B5 medium, pH 5.8 supplemented with 280 mM sucrose. To transfect protoplasts, 5-μg plasmid DNA was added to 5×10^5 protoplasts (in 50 μl volume) following the addition of 150 μl of transfection reagent (25% polyethylene glycol 6000, 450 mM mannitol, and 100 mM calcium nitrate). For the BiFC experiments 5 μg of pBiFCt-TPN1^{WT}/TPN1^{G163E} – nYFP + cYFP-RABH1b was used and 5 μg of pBiFCt-nYFP + cYFP-RABH1b or pBiFCt-2 in 1-CN (empty plasmid) were used as negative controls. For colocalization experiments 2.5 μg each of pHGW-*RABH1b*$_{pro}$:*GFP-RABh1b* and pGreen-*TPN1*$_{pro}$:*TPN1*^{WT}/*TPN1*^{G163E}-*mCherry* were used. After 30 min of incubation, the protoplasts were washed twice with 275 mM calcium nitrate and finally incubated in Gamborgs B5 medium pH 5.8, supplemented with 340 mM glucose + 340 mM mannitol and 100 μg/ml ampicillin. Protoplasts were imaged 30 h post transfection. For BiFC experiment only RFP-positive protoplasts were imaged. For YFP/RFP fluorescence ratio calculation, fluorescent intensity was measured from maximum intensity Z projection of protoplasts in YFP and RFP channels using Fiji/ImageJ.

Fluorescence lifetime measurement

Fluorescence lifetime of GFP was measured by microscopy coupled with time-correlated single photon counting (TCSPC). Protoplasts expressing *RABH1b*$_{pro}$:*GFP-RABh1b*, *RABH1b*$_{pro}$:*GFP-RABh1b* + *TPN1*$_{pro}$:*TPN1*^{WT}-*mCherry* and *RABH1b*$_{pro}$:*GFP-RABh1b* + *TPN1*$_{pro}$:*TPN1*^{G163E}-*mCherry* were imaged with Zeiss LSM880 confocal microscope coupled with a FLIM Upgrade Kit for laser scanning miscroscopy (PicoQuant GmbH, Germany), including PicoQuant pulsed diode lasers and HyD single-molecule detectors for photon detection and counting. Fluorescence lifetime parameters were extracted from whole protoplasts using the SymPhoTime 64 software (SPT64, PicoQuant GmbH, Germany). Fluorescence lifetime fitting on the lifetime decay curves revealed that the best fits could be obtained using 3 exponentials. Laser repetition rate was set to 40 MHz, and images were taken with 16.2 μs per pixel. A series of at least 10 frames were merged into one image and further analyzed.

CHC immunostaining

Fluorescent immunostaining was performed using whole mounts of roots from 5-d-old Arabidopsis light-grown seedlings following the method described by Pasternak et al. (2015) using 2% (v/v) formaldehyde fixation. Rabbit anti-CHC (Agrisera, catalogue no: AS10690) and DyLight 633 coupled donkey anti-rabbit (Jackson ImmunoResearch, catalogue no: NBP1-75638) were used in 1:500 and 1:1,000 dilutions, respectively. Nuclei of the cells were stained with 1 μg/ml solution of 4′,6-diamidino-2-phenylindole (DAPI) in distilled water. Samples were mounted in Citiflour AF1 antifade solution.

Ruthenium red staining of seed coat

Seed coat staining was performed following the method described by McFarlane et al. (2013). About 50 dry seeds/genotype were hydrated in deionized water containing 50 mM ethylenediaminetetraacetic acid pH 7.0 at room temperature for 1 h with gentle shaking (60 rpm). The solution was then aspirated and seeds were incubated in an 0.01% (w/v) aqueous solution of ruthenium red (Sigma-Aldrich) for 1 h After the incubation, the seeds were washed once in distilled water, mounted on glass slides and imaged using a Leica MZ9.5 stereomicroscope with Leica DC300 camera.

Confocal laser scanning microscopy

Samples were mounted in liquid one-half Murashige and Skoog media and imaged using a Zeiss 880 confocal microscope (40× water objective, numerical aperture 1.4). GFP, Venus, and DyLight633 were excited using 488, 514, and 633 nm laser lines, and their respective fluorescence were collected in the ranges of 495 to 540, 520 to 560, and 640 to 670 nm, respectively. mKO, RFP, & mCherry were excited using a 561-nm laser line and the emission of mKO was collected in the range of 570 to 640 nm, and that of RFP and mCherry in the range of 590 to 650 nm. A pinhole diameter of 1 airy unit, and system-optimized zoom settings were used for imaging.

Quantification of colocalization

Colocalization analysis for endomembrane compartments was done by optical section at the midplane of the cell. Colocalization analysis was performed using the centroid distance-based method as described previously (Boutté et al. 2013). Punctate structures in individual fluorescence channels were identified by the (2D/3D) particle tracker tool of ImageJ/Fiji and their centroid coordinates were recorded. Two particles were considered colocalized if their centroids were within the optical resolution limit (0.6λ/N.A), where λ is the wavelength of the longer emission fluorophore and N.A is the numerical aperture of the objective.

Quantification of RAB-GTPase compartments

For quantification of GFP-RABH1b/YFP-RABA1e/mCherry-RABA5d/RFP-RABE1d compartments, optical sections at the midplane of the cells were analyzed. Particles 10 to 20 pixels in diameter and in the upper 20th intensity percentile were counted using the particle tracker plugin of Fiji/ImageJ.

Total membrane fraction extraction and western blot analysis for AUX1-YFP

Seedlings expressing AUX1-YFP in WT, *ech* and *ech*; *TPN1*$_{pro}$:*TPN1*^{G163E} backgrounds as well as nontransgenic Col-0 and YFP-MEMBRIN12 were grown in the dark in liquid half Murashige and Skoog medium with 1% (w/v) sucrose and 2.5 mM morpholinoethanesulfonic acid (pH 5.8) for 7 d. Dark-grown seedlings were ground in extraction buffer (0.45 M sucrose, 5 mM MgCl2, 1 mM dithiothreitol, and 0.5% (w/v) Polyvinylpyrrolidone dissolved in 50 mM HEPES of pH 7.5), according to the protocol described in Ito et al. (2021). The supernatant was deposited on a 38% (w/v) sucrose cushion and then ultra-centrifuged for 2 h at 27,000 rpm. The membrane fraction floating at the interface of the sucrose cushion and supernatant was transferred in a new tube and diluted into 2 volumes of 50 mM HEPES (pH 7.5). After ultra-centrifugation at 27,000 rpm for 2 h, the supernatant was discarded and the pellet resuspended in 200 μL of Wash Buffer (0.25 M sucrose, 1.5 mM MgCl2, 0.2 mM EDTA, and 150 mM NaCl dissolved in 50 mM HEPES of pH 7.5) with the addition of 1 mM Phenylmethylsulfonyl Fluoride and protease inhibitor cocktail (Sigma-Aldrich), as described in Ito et al. (2021).

Total protein concentration in isolated membrane fractions was measured using the Bicinchronic Acid method. Before loading the gel, the samples were resuspended in Laemmli buffer and

incubated at 37 °C for 1 h. A total of 30 μg of protein was loaded per well of a 10% Mini-PROTEAN TGX Stain-Free polyacrylamide gel (BioRad). After migration, the gel was imaged under ultraviolet light to ensure equal loading of the fractions. Proteins were then electrophoretically transferred to a polyvinylidene difluoride membrane. The membrane was probed with rabbit anti-GFP (Merck catalogue no 11814460001, 1:1,000 dilution) as a proxy for AUX1-YFP and horse radish peroxidase-conjugated goat anti-rabbit IgG (BioRad catalogue no: 1706516, 1:3,000 dilution). Band intensities were quantified using ImageJ.

Statistical analysis

Statistical analysis was performed using RStudio software. The normality of the data was checked by Kolmogorov–Smirnov test and equality of variance was checked by Levene's test. Data were compared either by two-tailed *t*-test or one-way ANOVA followed by post hoc Tukey's test. For nonnormal datasets, groups of data were compared using the Kruskal–Wallis *H* test followed by the post hoc Mann–Whitney *U* test with Bonferroni correction. Details of statistical analysis, number of quantified entities (*n*), and measures of dispersion are mentioned in the figure legends. Statistical data are provided in Supplementary Data Set 1.

Accession numbers

Sequence data from this article can be found in the Arabidopsis Genome Initiative or GenBank/EMBL databases under the following accession numbers: TPN1 (At5g26740), TPN2 (At3g05940), ECH (At1g09330), RABH1a (At5g64990), RABH1b (At2g44610), RABH1c (At4g39890), RABH1d (At2g22290), RABH1e (At5g10260) VTI12 (At1g26670), CLC2 (At2g40060), AUX1 (At2g38120), RABA5d (At2g31680), RABA1e (At4g18430), RABE1d (At5g03520), SYP32 (At3g24350), MEMBRIN12 (At5g50440), and TUA3 (At5g19770).

Acknowledgments

We sincerely thank Daniël Van Damme and Kristoffer Jonsson for useful comments on the manuscript and László Bakó for providing *Arabidopsis* suspension culture cells.

Author contributions

A.B., D.G., Y.B., and R.P.B. designed the research. D.G. performed EMS suppressor screen of the *ech* mutant. B.A. performed the BiFC experiments and parts of the hook measurements. C.O., Ta.U., and To.U. provided the *rab1a*, *rabh1b*, *rabh1c*, *rabh1d*, and *ranh1e* mutants, the *RABH1b*$_{pro}$*:GFP-RABH1b* reporter line and provided valuable inputs. L.F. performed the microsomal membrane isolation and western blot experiments and lysotracker red staining/imaging. B.S. cloned the Venus tagged TPN1 genes. L.M.D.F. and P.M. measured and analyzed GFP lifetime. A.B. performed all the other experiments and analyzed data. A.B., Y.B., and R.P.B. wrote the paper. All authors read and approved the submission.

Supplementary data

The following materials are available in the online version of this article.

Supplementary Figure S1. Suppression of various *ech* phenotypes by TPN1^{G163E} (supports Fig. 1).

Supplementary Figure S2. The *ech* hook phenotype is not suppressed by transformation with TPN1^{WT} (supports Fig. 1).

Supplementary Figure S3. Amino acid sequence alignment and topology of TPN1 and TPN2 (supports Fig. 3).

Supplementary Figure S4. *ech* hook phenotype is suppressed by TPN2^{G163E} (supports Fig. 3)

Supplementary Figure S5. Membrane association of AUX1-YFP protein (supports Fig. 1).

Supplementary Figure S6. TPN1 protein does not localize to the Golgi (supports Fig. 2).

Supplementary Figure S7. TPN1^{WT} is mislocalized to vacuoles in apical hook cells in *ech* mutant (supports Fig. 2).

Supplementary Figure S8. Localization of TPN1^{G163E}-Venus in wild type and *ech* mutant root cells (supports Fig. 2).

Supplementary Figure S9. Characterization of *tpn1* and *tpn2* T-DNA mutants (supports Fig. 3).

Supplementary Figure S10. Phenotype of *ech tpn1* and *ech tpn2* double mutants (supports Fig. 3).

Supplementary Figure S11. Apical hook phenotype of *rabh1* mutants (supports Fig. 4).

Supplementary Figure S12. Localization of RAB-GTPases in wild type vs *ech* hook region epidermal cells (supports Fig. 4).

Supplementary Figure S13. Bimolecular Fluorescence Complementation (BiFC) between RABH1b and TPN1 (supports Fig. 4).

Supplementary Figure S14. Colocalization of RABH1b and TPN1 (supports Fig. 4).

Supplementary Figure S15. Effect of *rabh1b* on *ech*; TPN1^{G163E} plant phenotype (supports Fig. 4).

Supplementary Figure S16. Genetic interaction of RABH1b and TPNs in apical hook development (supports Fig. 4).

Supplementary Table S1. Cloning and genotyping primers.

Supplementary Data Set 1. Summary of statistical tests.

Funding

This work was funded by grants from Knut and Alice Wallenberg Foundation, Sweden (Grant ID: 20120050) awarded to R.P.B.

Conflict of interest statement. None declared.

Data availability

The data underlying this article will be shared on reasonable request to the corresponding author.

References

Asaoka R, Uemura T, Ito J, Fujimoto M, Ito E, Ueda T, Nakano A. Arabidopsis RABA1 GTPases are involved in transport between the trans-Golgi network and the plasma membrane, and are required for salinity stress tolerance. *Plant J*. 2013:73(2):240–249. https://doi.org/10.1111/tpj.12023

Boutté Y, Jonsson K, McFarlane HE, Johnson E, Gendre D, Swarup R, Friml J, Samuels L, Robert S, Bhalerao RP. ECHIDNA-mediated post-Golgi trafficking of auxin carriers for differential cell elongation. *Proc Natl Acad Sci U S A*. 2013:110(40):16259–16264. https://doi.org/10.1073/pnas.1309057110

Chow CM, Neto H, Foucart C, Moore I. Rab-A2 and Rab-A3 GTPases define a trans-Golgi endosomal membrane domain in Arabidopsis that contributes substantially to the cell plate. *Plant Cell*. 2008:20(1):101–123. https://doi.org/10.1105/tpc.107.052001

Clough SJ, Bent AF. Floral dip: a simplified method for Agrobacterium-mediated transformation of *Arabidopsis thaliana*. *Plant J*. 1998:16(6):735–743. https://doi.org/10.1046/j.1365-313x.1998.00343.x

Drakakaki G, Ven W, Pan S, Miao Y, Wang J, Keinath NF, Weatherly B, Jiang L, Schumacher K, Hicks G, et al. Isolation and proteomic analysis of the SYP61 compartment reveal its role in exocytic trafficking in Arabidopsis. *Cell Res*. 2012:22(2):413–424. https://doi.org/10.1038/cr.2011.129

Feraru E, Feraru MI, Asaoka R, Paciorek T, Rycke R, Tanaka H, Nakano A, Friml J. BEX5/RabA1b regulates trans-Golgi network-to-plasma membrane protein trafficking in Arabidopsis. *Plant Cell*. 2012:24(7):3074–3086. https://doi.org/10.1105/tpc.112.098152

Fuji K, Shirakawa M, Shimono Y, Kunieda T, Fukao Y, Koumoto Y, Takahashi H, Hara-Nishimura I, Shimada T. The adaptor complex AP-4 regulates vacuolar protein sorting at the trans-Golgi network by interacting with VACUOLAR SORTING RECEPTOR1. *Plant Physiol*. 2016:170(1):211–219. https://doi.org/10.1104/pp.15.00869

Fülöp K, Pettkó-Szandtner A, Magyar Z, Miskolczi P, Kondorosi É, Dudits D, Bakó L. The *Medicago* CDKC;1-CYCLINT;1 kinase complex phosphorylates the carboxy-terminal domain of RNA polymerase II and promotes transcription. *Plant J*. 2005:42(6):810–820. https://doi.org/10.1111/j.1365-313X.2005.02421.x

Geldner N, Dénervaud-Tendon V, Hyman DL, Mayer U, Stierhof YD, Chory J. Rapid, combinatorial analysis of membrane compartments in intact plants with a multicolor marker set. *Plant J*. 2009:59(1):169–178. https://doi.org/10.1111/j.1365-313X.2009.03851.x

Gendre D, Jonsson K, Boutté Y, Bhalerao RP. Journey to the cell surface–the central role of the trans-Golgi network in plants. *Protoplasma*. 2015:252(2):385–398. https://doi.org/10.1007/s00709-014-0693-1

Gendre D, McFarlane HE, Johnson E, Mouille G, Sjödin A, Oh J, Levesque-Tremblay G, Watanabe Y, Samuels L, Bhalerao RP. Trans-Golgi network localized ECHIDNA/Ypt interacting protein complex is required for the secretion of cell wall polysaccharides in Arabidopsis. *Plant Cell*. 2013:25(7):2633–2646. https://doi.org/10.1105/tpc.113.112482

Gendre D, Oh J, Boutte Y, Best JG, Samuels L, Nilsson R, Uemura T, Marchant A, Bennett MJ, Grebe M, et al. Conserved Arabidopsis ECHIDNA protein mediates trans-Golgi-network trafficking and cell elongation. *Proc Natl Acad Sci U S A*. 2011:108(19):8048–8053. https://doi.org/10.1073/pnas.1018371108

Grefen C, Blatt MR. A 2in1 cloning system enables ratiometric bimolecular fluorescence complementation (rBiFC). *Biotechniques*. 2012:53(5):311–314. https://doi.org/10.2144/000113941

He M, Lan M, Zhang B, Zhou Y, Wang Y, Zhu L, Yuan M, Fu Y. Rab-H1b is essential for trafficking of cellulose synthase and for hypocotyl growth in *Arabidopsis thaliana*. *J Integr Plant Biol*. 2018:60(11):1051–1069. https://doi.org/10.1111/jipb.12694

Heinze L, Freimuth N, Rößling AK, Hahnke R, Riebschläger S, Fröhlich A, Sampathkumar A, McFarlane HE, Sauer M. EPSIN1 and MTV1 define functionally overlapping but molecularly distinct trans-Golgi network subdomains in Arabidopsis. *Proc Natl Acad Sci U S A*. 2020:117(41):25880–25889. https://doi.org/10.1073/pnas.2004822117

Ikeda Y, Men S, Fischer U, Stepanova AN, Alonso JM, Ljung K, Grebe M. Local auxin biosynthesis modulates gradient-directed planar polarity in Arabidopsis. *Nat Cell Biol*. 2009:11(6):731–738. https://doi.org/10.1038/ncb1879

Ito E, Fujimoto M, Ebine K, Uemura T, Ueda T, Nakano A. Dynamic behavior of clathrin in *Arabidopsis thaliana* unveiled by live imaging. *Plant J*. 2012:69(2):204–216. https://doi.org/10.1111/j.1365-313X.2011.04782.x

Ito Y, Esnay N, Platre MP, Wattelet-Boyer V, Noack LC, Fougère L, Menzel W, Claverol S, Fouillen L, Moreau P, et al. Sphingolipids mediate polar sorting of PIN2 through phosphoinositide consumption at the trans-Golgi network. *Nat Commun*. 2021:12(1):4267. https://doi.org/10.1038/s41467-021-24548-0

Jonsson K, Boutté Y, Singh RK, Gendre D, Bhalerao RP. Ethylene regulates differential growth via BIG ARF-GEF-dependent post-Golgi secretory trafficking in Arabidopsis. *Plant Cell*. 2017:29(5):1039–1052. https://doi.org/10.1105/tpc.16.00743

Karimi M, Inzé D, Depicker A. GATEWAY vectors for Agrobacterium-mediated plant transformation. *Trends Plant Sci*. 2002:7(5):193–195. https://doi.org/10.1016/S1360-1385(02)02251-3

Kranjc T, Dempsey E, Cagney G, Nakamura N, Shields DC, Simpson JC. Functional characterisation of the YIPF protein family in mammalian cells. *Histochem Cell Biol*. 2017:147(4):439–451. https://doi.org/10.1007/s00418-016-1527-3

Lutz KA, Wang W, Zdepski A, Michael TP. Isolation and analysis of high quality nuclear DNA with reduced organellar DNA for plant genome sequencing and resequencing. *BMC Biotechnol*. 2011:11(1):54. https://doi.org/10.1186/1472-6750-11-54

Mathur J, Koncz C. PEG-Mediated protoplast transformation with naked DNA. In: Martinez-Zapater JM, Salinas J, editors. *Arabidopsis protocols*. Totowa (NJ): Humana Press; 1998. p. 267–276.

McFarlane HE, Watanabe Y, Gendre D, Carruthers K, Levesque-Tremblay G, Haughn GW, Bhalerao RP, Samuels L. Cell wall polysaccharides are mislocalized to the vacuole in echidna mutants. *Plant Cell Physiol*. 2013:54(11):1867–1880. https://doi.org/10.1093/pcp/pct129

Olivier-Mason A, Wojtyniak M, Bowie RV, Nechipurenko IV, Blacque OE, Sengupta P. Transmembrane protein OSTA-1 shapes sensory cilia morphology via regulation of intracellular membrane trafficking in *C. elegans*. *Development*. 2013:140(7):1560–1572. https://doi.org/10.1242/dev.086249

Pasternak T, Tietz O, Rapp K, Begheldo M, Nitschke R, Ruperti B, Palme K. Protocol: an improved and universal procedure for whole-mount immunolocalization in plants. *Plant Methods*. 2015:11(1):50. https://doi.org/10.1186/s13007-015-0094-2

Pfeffer SR. Rab GTPases: master regulators that establish the secretory and endocytic pathways. *Mol Biol Cell*. 2017:28(6):712–715. https://doi.org/10.1091/mbc.e16-10-0737

Qi X, Zheng H. Rab-A1c GTPase defines a population of the trans-Golgi network that is sensitive to endosidin1 during cytokinesis in Arabidopsis. *Mol Plant*. 2013:6(3):847–859. https://doi.org/10.1093/mp/sss116

Renna L, Brandizzi F. The mysterious life of the plant trans-Golgi network: advances and tools to understand it better. *J Microsc*. 2020:278(3):154–163. https://doi.org/10.1111/jmi.12881

Renna L, Stefano G, Slabaugh E, Wormsbaecher C, Sulpizio A, Zienkiewicz K, Brandizzi F. TGNap1 is required for microtubule-dependent homeostasis of a subpopulation of the plant trans-Golgi network. *Nat Commun*. 2018:9(1):5313. https://doi.org/10.1038/s41467-018-07662-4

Rios AF, Radoeva T, De Rybel B, Weijers D, Borst JW. FRET-FLIM for visualizing and quantifying protein interactions in live plant cells. *Methods in Molecular Biology*. 2017:1497:135–146. https://doi.org/10.1007/978-1-4939-6469-7_13

Rosquete MR, Davis DJ, Drakakaki G. The plant trans-Golgi network: not just a matter of distinction. *Plant Physiol*. 2018:176(1):187–198. https://doi.org/10.1104/pp.17.01239

Schneeberger K, Ossowski S, Lanz C, Juul T, Petersen AH, Nielsen KL, Jorgensen JE, Weigel D, Andersen SU. SHOREmap: simultaneous mapping and mutation identification by deep sequencing. *Nat Methods*. 2009:6(8):550–551. https://doi.org/10.1038/nmeth0809-550

Shimizu Y, Takagi J, Ito E, Ito Y, Ebine K, Komatsu Y, Goto Y, Sato M, Toyooka K, Ueda T, et al. Cargo sorting zones in the trans-Golgi network visualized by super-resolution confocal live imaging

microscopy in plants. *Nat Commun*. 2021:12(1):1901. https://doi.org/10.1038/s41467-021-22267-0

Sivars U, Aivazian D, Pfeffer SR. Yip3 catalyses the dissociation of endosomal Rab-GDI complexes. *Nature*. 2003:425(6960):856–859. https://doi.org/10.1038/nature02057

Speth EB, Imboden L, Hauck P, He SY. Subcellular localization and functional analysis of the Arabidopsis GTPase RabE. *Plant Physiol*. 2009:149(4):1824–1837. https://doi.org/10.1104/pp.108.132092

Swarup R, Kargul J, Marchant A, Zadik D, Rahman A, Mills R, Yemm A, May S, Williams L, Millner P, et al. Structure-function analysis of the presumptive Arabidopsis auxin permease AUX1. *Plant Cell*. 2004:16(11):3069–3083. https://doi.org/10.1105/tpc.104.024737

Tanaka H, Kitakura S, Rakusová H, Uemura T, Feraru MI, De Rycke R, Robert S, Kakimoto T, Friml J. Cell polarity and patterning by PIN trafficking through early endosomal compartments in *Arabidopsis thaliana*. *PLoS Genet*. 2013:9(5):e1003540. https://doi.org/10.1371/journal.pgen.1003540

Vernoud V, Horton AC, Yang Z, Nielsen E. Analysis of the small GTPase gene superfamily of Arabidopsis. *Plant Physiol*. 2003:131(3):1191–1208. https://doi.org/10.1104/pp.013052

Viotti C, Bubeck J, Stierhof YD, Krebs M, Langhans M, Berg W, Dongen W, Richter S, Geldner N, Takano J. Endocytic and secretory traffic in Arabidopsis merge in the trans-Golgi network/early endosome, an independent and highly dynamic organelle. *Plant Cell*. 2010:22(4):1344–1357. https://doi.org/10.1105/tpc.109.072637

Wang P, Chen X, Goldbeck C, Chung E, Kang BH. A distinct class of vesicles derived from the trans-Golgi mediates secretion of xylogalacturonan in the root border cell. *Plant J*. 2017:92(4):596–610. https://doi.org/10.1111/tpj.13704

Wattelet-Boyer V, Brocard L, Jonsson K, Esnay N, Joubès J, Domergue F, Mongrand S, Raikhel N, Bhalerao RP, Moreau P, et al. Enrichment of hydroxylated C24- and C26-acyl-chain sphingolipids mediates PIN2 apical sorting at trans-Golgi network subdomains. *Nat Commun*. 2016:7(1):12788. https://doi.org/10.1038/ncomms12788

Wilkop T, Pattathil S, Ren G, Davis DJ, Bao W, Duan D, Peralta AG, Domozych DS, Hahn MG, Drakakaki G. A hybrid approach enabling large-scale glycomic analysis of post-Golgi vesicles reveals a transport route for polysaccharides. *Plant Cell*. 2019:31(3):627–644. https://doi.org/10.1105/tpc.18.00854

Zhang X, Zhao H, Gao S, Wang W-C, Katiyar-Agarwal S, Huang H-D, Raikhel N, Jin H. Arabidopsis argonaute 2 regulates innate immunity via miRNA393(*)-mediated silencing of a Golgi-localized SNARE gene, MEMB12. *Mol Cell*. 2011:42(3):356–366. https://doi.org/10.1016/j.molcel.2011.04.010

Zheng H, Zheng W, Wu C, Yang J, Xi Y, Xie Q, Zhao X, Deng X, Lu G, Li G, et al. Rab GTPases are essential for membrane trafficking-dependent growth and pathogenicity in *Fusarium graminearum*. *Environ Microbiol*. 2015:17(11):4580–4599. https://doi.org/10.1111/1462-2920.12982